Accepted for Publication in ApJS
Preprint typeset using LaTeX style emulateapj v. 11/26/04

THE ACS FORNAX CLUSTER SURVEY. I. INTRODUCTION TO THE SURVEY AND DATA REDUCTION PROCEDURES[1]

Andrés Jordán[2], John P. Blakeslee[3], Patrick Côté[4], Laura Ferrarese[4], Leopoldo Infante[5], Simona Mei[6], David Merritt[7], Eric W. Peng[4], John L. Tonry[8], Michael J. West[9,10]

Accepted for Publication in ApJS

ABSTRACT

The Fornax Cluster is a conspicuous cluster of galaxies in the southern hemisphere and the second largest collection of early-type galaxies within $\lesssim 20$ Mpc after the Virgo Cluster. In this paper, we present a brief introduction to the ACS Fornax Cluster Survey — a program to image, in the F475W (g_{475}) and F850LP (z_{850}) bandpasses, 43 early-type galaxies in Fornax using the *Advanced Camera for Surveys* (ACS) on the *Hubble Space Telescope*. Combined with a companion survey of Virgo, the ACS Virgo Cluster Survey, this represents the most comprehensive imaging survey to date of early-type galaxies in cluster environments in terms of depth, spatial resolution, sample size and homogeneity. We describe the selection of the program galaxies, their basic properties, and the main science objectives of the survey which include the measurement of luminosities, colors and structural parameters for globular clusters associated with these galaxies, an analysis of their isophotal properties and surface brightness profiles, and an accurate calibration of the surface brightness fluctuation distance indicator. Finally, we discuss the data reduction procedures adopted for the survey.

Subject headings: galaxies: clusters: individual (Fornax) — galaxies: elliptical and lenticular, cD — galaxies: distances and redshifts — galaxies: star clusters — galaxies: nuclei — methods: data analysis

1. INTRODUCTION

Much of our current understanding of galaxy formation and evolution is based on observations of galaxies in cluster environments. While not necessarily representative of clusters at high redshift, nearby clusters have played a key role in shaping this understanding for the simple reason that they are amenable to study in a level of detail that will never be possible for the more distant systems.

Among the nearby clusters, Virgo is almost certainly the most thoroughly studied. Indeed, it can probably be said that Virgo is the most closely examined cluster of galaxies in the entire universe (see, e.g., the discussions in Huchra 1985; Binggeli, Sandage & Tammann 1985; Binggeli 1999; Gavazzi et al. 2003; Côté et al. 2004). After Virgo, the largest concentration of galaxies within $\lesssim 20$ Mpc of our galaxy is the Fornax cluster. This cluster, the most conspicuous concentration of galaxies in the southern hemisphere, is centered roughly at $\alpha \sim 3^{\rm h}35^{\rm m}$ and $\delta \sim -35.7°$ (Ferguson 1989a). It is located in the Fornax constellation, which was introduced in the 18th century by the Abbé Nicolas Louis de la Caille while mapping the southern skies from the Cape of Good Hope during the years 1751–1753[11].

To the best of our knowledge, it was first identified as a bonafide galaxy cluster by Shapley (1943) who compiled data on many of the most prominent members and wrote "Table 3 lists some of the information we have at hand concerning a score of bright objects in the constellation Fornax, which are so located with respect to one another that the law of chance is hard pressed if these objects are only accidentally near together. They appear to constitute a real colony of galaxies, mutually operating.". However, a complete census of cluster members was still many years away, and even as late as 1956, NGC 1399 — the luminous cD/E0 galaxy at the dynamical center of the main component of the cluster (Drinkwater, Gregg & Colless 2001a) — was listed as a non-cluster galaxy in the catalog of Humason, Mayall & Sandage (1956).

Studies of the Fornax cluster have often followed on the heels of similar studies of the Virgo cluster. For instance, one of the first studies of Fornax reported the discovery of dwarf galaxies (Hodge 1959) after a similar population had been uncovered in Virgo by Reaves (1956). The earliest catalogs of Fornax cluster members

[1] Based on observations with the NASA/ESA *Hubble Space Telescope* obtained at the Space Telescope Science Institute, which is operated by the Association of Universities for Research in Astronomy, Inc., under NASA contract NAS 5-26555
[2] European Southern Observatory, Karl-Schwarzschild-Str. 2, 85748 Garching bei München, Germany; ajordan@eso.org
[3] Department of Physics and Astronomy, Washington State University, 1245 Webster Hall, Pullman, WA 99163-2814
[4] Herzberg Institute of Astrophysics, Victoria, BC V9E 2E7, Canada
[5] Departamento de Astronomía y Astrofísica, Pontificia Universidad Católica de Chile, Avenida Vicuña Mackenna 4860, Casilla 306, Santiago 22, Chile
[6] GEPI, Observatoire de Paris, Section de Meudon, 5 place Jules Janssen, 92195 Meudon Cedex, France
[7] Department of Physics, Rochester Institute of Technology, 84 Lomb Memorial Drive, Rochester, NY 14623
[8] Institute for Astronomy, University of Hawai'i, 2680 Woodlawn Drive, Honolulu, HI 96822
[9] Department of Physics & Astronomy, University of Hawai'i, Hilo, HI 96720
[10] Gemini Observatory, Casilla 603, La Serena, Chile

[11] The Fornax constellation was originally named "Le Fourneau", later latiniced to "Fornax Chimiae" (Chemical Furnace). In the spirit of the illustration de la Caille named several constellations after instruments of the liberal and philosophical arts. He gave us also 'Apparatus Sculptoris' (sculptor's apparatus, now Sculptor) and 'Antlia Pneumatica' (air pump, now Antlia), among others. See Evans (1951) for a brief account of La Caille's work in the Cape.

(Hodge 1960, Hodge, Pyper & Webb 1965) were eventually supplanted by the Fornax Cluster Catalog (FCC) of Ferguson (1989a), who surveyed 40 square degrees using large-scale plates from the 2.5m Las Campanas telescope — the same telescope that was used some years before to assemble the Virgo Cluster Catalog (Binggeli et al. 1985). The FCC remains the most comprehensive catalog of Fornax currently available.

The globular cluster systems of the brightest Fornax galaxies were first tentatively detected around NGC 1374, NGC 1379, and NGC 1399 by carrying out starcounts in a single deep photographic plate (Dawe & Dickens 1975), a full two decades after a similar population had been first discussed for M87, the giant elliptical in the center of the Virgo cluster (Baum 1955). A systematic study of globular cluster systems in Fornax was later presented by Hanes & Harris (1986) as one of a series of papers on extragalactic globular clusters (which had included the study of globular clusters in Virgo galaxies in previous installments).

In the all-important task of establishing the cosmological distance ladder, Cepheids were used by the HST Key Project on the Extragalactic Distance Scale to derive a distance to Fornax (Madore et al. 1999) shortly after the same program had identified Cepheids in Virgo (Freedman et al. 1994; Ferrarese et al. 1996). Following initial feasibility tests of the surface brightness fluctuations (SBF; Tonry & Schneider 1988) distance indicator on M32 and NGC 3379, the method was applied to a significant number of galaxies in the Virgo Cluster (Tonry, Ajhar & Luppino 1989, 1990). However, because of complications arising from the significant line-of-sight depth of Virgo, the first accurate calibration of the SBF method had to await subsequent observations of galaxies in the Fornax cluster (Tonry 1991).

Despite their shared proximity to our Galaxy, the two clusters show some obvious differences that invite intercomparisons (see Table 1, which summarizes the basic properties of the clusters). It is clear both Fornax and Virgo offer a unique opportunity to examine the possible effects of environment on the properties of cluster galaxies. For instance, Fornax is far more regular in shape, and probably more dynamically evolved, than its northern counterpart. It is also considerably smaller and denser than Virgo, with a core radius $\sim 40\%$ that of Virgo and a central density twice as large. The total mass of Fornax is $\approx 7 \times 10^{13} M_{\odot}$, as estimated from galaxy radial velocities (Drinkwater et al. 2001a), which is $\sim 1/10$ that of Virgo. Fornax is thus more representative of the groups and poor clusters in which most galaxies in the universe reside.

Being a much more compact cluster than Virgo, Fornax is an ideal target for the calibration of distance indicators (see above). However, like most clusters, it does show some substructure — the main subcluster is centered on NGC 1399, while a subcluster that includes NGC 1316 (= Fornax A) is centered 3° to the southwest (Drinkwater et al. 2001a). Within the main subcluster, there seems to be an infalling clump associated with NGC 1404, a picture that is supported by the characteristics of its X-ray emission (Scharf et al. 2005, Machacek et al. 2005).

The installation of the Advanced Camera for Surveys (ACS; Ford et al. 1998) on board the *Hubble Space Telescope* (HST) improved dramatically the telescope's imaging capabilities. In the first cycle of operations with ACS, we initiated the ACS Virgo Cluster Survey (ACSVCS; Côté et al. 2004), a program to obtain deep F475W ($\approx$ Sloan g) and F850LP ($\approx$ Sloan z) ACS/WFC images for 100 early-type members of the Virgo cluster. As the second step in a broader program to obtain high-resolution imaging for a large, well-defined sample of early-type galaxies in nearby clusters, we initiated the ACS Fornax Cluster Survey (ACSFCS). This ACS/WFC survey of 43 early-type galaxies in the Fornax cluster was carried out using the same observational strategy that was employed in the ACSVCS. Collectively, these two surveys provide homogeneous g_{475}- and z_{850}-band imaging of 143 galaxies with magnitudes $B_T \lesssim 16$, a dataset with wide-ranging scientific potential.

In this paper, the first in a series, we present an introduction to the ACSFCS and discuss the data reduction procedures adopted for it. The paper is organized as follows: we present a brief description of the survey objectives in §2, outline selection of sample galaxies in §3 and describe the observations in §4. We detail the data reduction procedures of the survey in §5 and conclude in §6.

2. MOTIVATION AND OBJECTIVES

The motivations for undertaking a high-spatial resolution, multi-wavelength imaging survey of galaxies in nearby clusters has been presented in the context of the ACSVCS by Côté et al. (2004). The survey images have a wide-ranging use for a variety of scientific applications, some of which were foreseen during the planning of the survey and some which were not. At the time of writing, the broad array of scientific results from the ACSVCS have been reported in sixteen refereed papers[12].

As mentioned above, the Fornax cluster provides a unique counterpart to Virgo in terms of environment; e.g., studies that were carried out in Virgo can be extended to Fornax, both increasing the total sample size and allowing the search for effects that cluster environment may have on findings based on the richer and less dense Virgo cluster. It is not our intention to provide a thorough review of the background of each science objective of the present survey. Instead, we will briefly discuss four main scientific topics that will be addressed using this new dataset. The interested reader is referred to the published papers from the ACSVCS for detailed references and results.

2.1. *Extragalactic Globular Clusters*

A key objective of the ACSFCS is the study of thousands of globular clusters (GCs) associated with the program galaxies. The images are sufficiently deep that $\sim 90\%$ of the GCs falling within the ACSFCS fields can be detected at a high level of completeness (Côté et al. 2004). Moreover, the high spatial resolution of *HST* allows the measurement the half-light radii for GCs by fitting point spread function (PSF)-convolved models to the two-dimensional light distributions (Jordán et al. 2005). As part of the analysis (see below), we classify and analyze sources in several control fields to obtain an accurate estimate of the expected contamination for each

[12] See the ACSVCS website: http://www.cadc.hia.nrc.gc.ca/community/ACSVCS

TABLE 1
Basic Data for the Virgo and Fornax Clusters.

Property (1)	Virgo (2)	Fornax (3)	References (4)
Richness Class	1	0	1,2
B-M Type	III	I	1,2
Mass	$(4\text{–}7)\times10^{14}M_\odot$	$(7\pm2)\times10^{13}M_\odot$	3,4,5
Distance (Mpc)	16.5	19.3	6,7
$\langle v_r\rangle$ (km sec^{-1})	1094 ± 42	1493 ± 36	5,8
σ_v (km sec^{-1})	760	374 ± 26	5,8
r_c (Mpc)	≈0.6	≈0.25	9
n_0 (gal Mpc^{-3})	≈250	≈500	9
N	1170	235	9
$f_{\rm E+dE+S0+dS0}$	0.8	0.87	9
$\langle kT\rangle_X$ (keV)	2.58 ± 0.03	1.20 ± 0.04	10
$\langle{\rm Fe}\rangle_X$ (solar)	0.34 ± 0.02	0.23 ± 0.03	10

Note. — Key to columns—(1) Cluster properties listed in the Table are the richness class, Bautz-Morgan (B-M) Type, mass, distance, average heliocentric radial velocity $\langle v_r\rangle$, velocity dispersion σ_v, King model core radius r_c, central galaxy density n_0, number of members N with $B\lesssim18$ and within $3.5r_c$, the fraction of these that are E, dE, S0 or dS0 ($f_{\rm E+dE+S0+dS0}$), and the average temperature, $\langle kT\rangle_X$, and Fe abundance, $\langle{\rm Fe}\rangle_X$, of the intracluster medium as derived from X-ray observations (excluding the inner cluster regions); (2-3) Value of given property for the Virgo and Fornax clusters respectively; (4) Reference for quoted value: 1.- Abell, Corwin & Olowin 1989; 2.- Girardi et al. 1995; 3.- McLaughlin 1999; 4.- Tonry et al. 2000; 5.- Drinkwater et al. 2001b; 6.- Mei et al. 2007; 7.- Tonry et al. 2001; 8.- Binggeli, Sandage & Tamman 1987; 9.- Ferguson 1989b; 10.- Fukazawa et al. 1997.

galaxy in the survey (Peng et al. 2006ab; Jordán et al. 2007, in preparation).

GC catalogs for each galaxy, combined with similar information for the likely contaminants, will be used to study the color distribution of GCs (cf. Peng et al. 2006a), their distribution of sizes (cf Jordán et al. 2005), their luminosity functions (cf. Jordán et al. 2006; 2007) and their distribution within the color-magnitude diagram (cf. Mieske et al. 2006b). With the addition of many new Fornax galaxies, it will be possible to take a first look into the role played by environment in shaping the overall properties of GC systems. The ACSFCS observations will also provide a direct test of the accuracy of the median GC half-light radii as a standard ruler for distance estimation (Jordán et al. 2005). We note that the sizes of GCs surrounding NGC 1399 derived from the ACSFCS data have already been used by Mieske et al. (2006a) to provide additional evidence for the onset of a GC mass-size relation at masses of $M\gtrsim2\times10^6M_\odot$, as originally suggested by Haşegan et al. (2005).

It had been recognized since the early days of X-ray astronomy that GCs are highly efficient in producing low-mass X-ray binaries (LMXBs; Clark 1975; Katz 1975). Thanks to the excellent imaging capabilities of Chandra and HST, tremendous progress has been made in recent years on the connection between LMXBs and GCs in external galaxies as distant as ~30 Mpc. Such studies have shed light on the processes that form LMXBs in dense GC environments and have also produced some surprising results, such as the fact that metal-rich GCs are ≈3 times more efficient at forming LXMBs than their metal-poor counterparts (see, e.g., Fabbiano 2006 and references therein). By combining new and archival data from *Chandra* with optical data from the ACSVCS we have carried out comprehensive studies of the connection between GCs and LMXBs in Virgo galaxies (Jordán et al. 2004a; Sivakoff et al. 2006). The ACSFCS data will enable such studies to be extended to the Fornax cluster.

2.2. *Surface Brightness Profiles and the Core Structure of Early-Type Galaxies*

Surface photometry and isophotal studies have historically played an important role in shaping our understanding of the origin and structure of early-type galaxies (see, e.g., Kormendy & Djorgovski 1989). In particular, high-resolution imaging from HST has made it possible to probe the innermost regions of nearby galaxies allowing the systematic study of brightness profiles down to scales of tens of parsecs. These inner profiles continue to hold much interest as it is now understood that the physical processes at the centers of galaxies — and, in particular, those related to the supermassive black holes (SBHs) thought to reside there (Ferrarese & Ford 2005) — are somehow connected to the history of the galaxy as a whole (e.g., Croton et al. 2006).

The ACSFCS data will be used to measure surface brightness profiles and perform a study of dust morphology and nuclear properties for galaxies in a new and different environment (cf. Ferrarese et al. 2006a, Côté et al. 2006). An interesting result that was unanticipated at the outset of the ACSVCS was the realization that previous ground-based studies of early-type galaxies had significantly underestimated the number of galaxies which contain compact stellar nuclei at, or near, their photocenters. It was found that ≈70–80% of the ACSVCS sample galaxies contained such nuclei, roughly three times higher than previously believed (Côté et al. 2006). This incidence of nucleation is similar to that found for late-type galaxies, which often contain a "nuclear star cluster" at, or near, their photocenters (e.g., Carollo et al. 1997, 1998; Matthews et al. 1999; Böker et al. 2002, 2004; Walcher et al. 2005; Seth et al. 2006).

The ACSVCS has allowed an exploration of the connection between core structure, stellar nuclei, and SBHs in new levels of detail. On subarcsecond scales (i.e., $r\sim0\farcs1$-$1''$, or $\sim$ 10-100 pc), the surface brightness profiles were found to vary systematically as one moves down the luminosity function (Ferrarese et al. 2006a; Côté

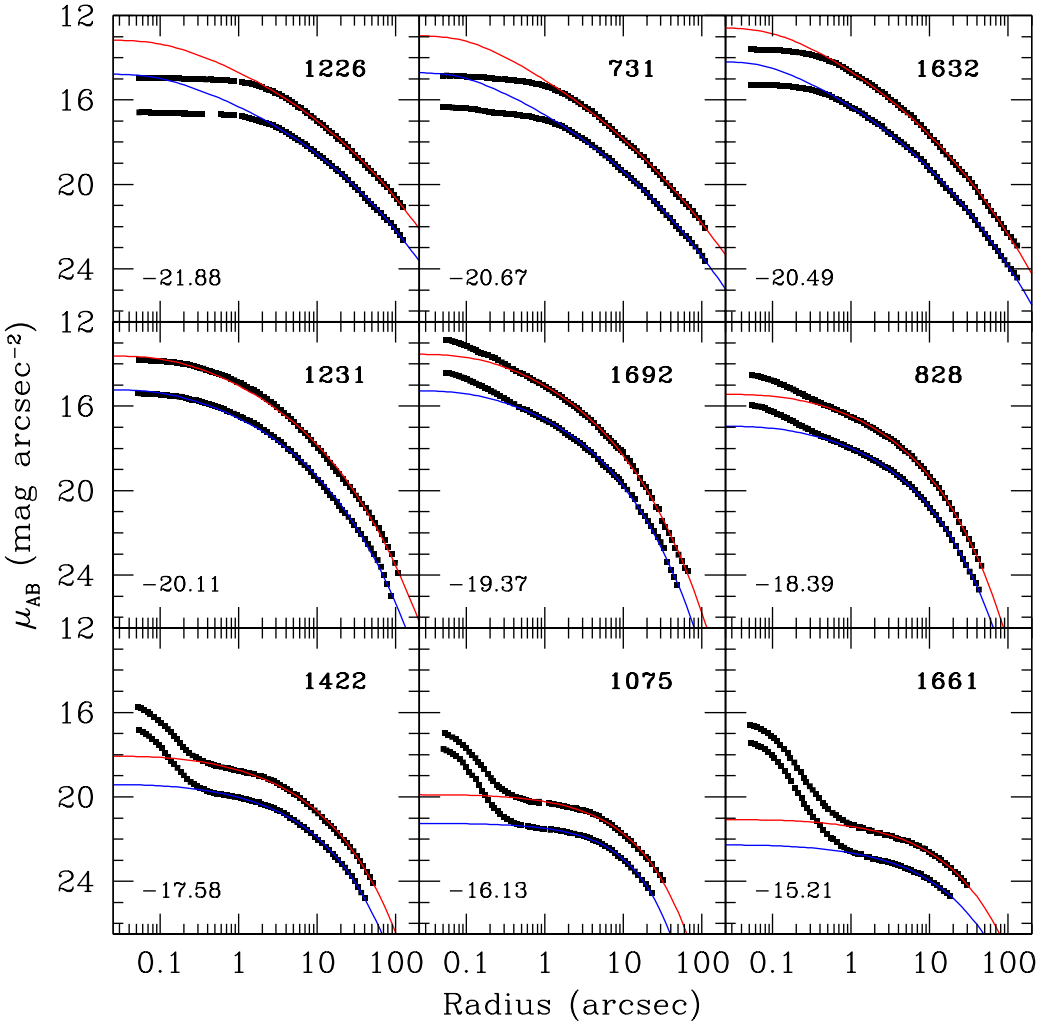

FIG. 1.— Representative surface brightness profiles for nine early-type galaxies from the ACSVCS spanning a factor of ~ 460 in blue luminosity; the $B-$band magnitude of each galaxy is listed in the corresponding panel. In each panel, we show the azimuthally-averaged brightness profile in the g_{475} and z_{850} bands plotted as a function of mean geometric radius (lower and upper profiles, respectively). The solid curves show Sérsic models fitted to the profiles beyond $\sim 0\farcs2$-$2''$. Note the gradual progression from a central light "deficit" to "excess", with a transition at $M_B \sim -20$ (see Ferrarese et al. 2006a and Côté et al. 2006 for details).

et al. 2006). Bright galaxies ($M_B \lesssim -20$), which in agreement with previous HST studies (e.g., Crane et al. 1993; Ferrarese et al. 1994; Lauer et al. 1995) exhibit a nearly constant surface brightness cores, have surface brightness profiles that fall below the inward extrapolation of the Sérsic model fitted beyond a few arcseconds (see also Graham et al. 2003). Meanwhile, progessively fainter galaxies show increasingly steep upturns over the Sérsic models that fit the galaxies on scales greater than $\sim 0\farcs1$-$1''$. In other words, on small (subarcsecond) angular scales, galaxies were found to exhibit a gradual progession from a light "deficit" to a light "excess" (see Figure 1), while on larger scales (i.e., $\gtrsim$ a few arcseconds), the curved brightness profiles of real galaxies (both giants and dwarfs) are accurately captured by Sérsic models, but not by the broken power-law parameterizations used in earlier studies (the "Nuker law", Lauer et al. 1995).

Stellar nuclei are consistenly absent only in the brightest galaxies — the same galaxies which are believed to host SBHs. In addition, it was found that nuclei in the low- and intermediate-mass galaxies contribute a mean fraction, $\eta \sim 0.2\%$, of the total galaxy luminosity (Côté et al. 2006, Ferrarese et al. 2006b). This fraction is, to within the errors, the same as the fractional *mass* contribution of the central SBHs in massive early-type galaxies (see also Rossa et al. 2006 for similar conclusions regarding nuclear star clusters in late-type galaxies). Long-slit, integrated-light spectra for several dozen galaxies in the ACSVCS were used to derive dynamical galaxy masses $\mathcal{M}_{\rm gal}$. Combining these masses with masses for the nuclei derived from the brightness profiles and stellar population models, it was found that a single $\mathcal{M}_{\rm CMO}$-$\mathcal{M}_{\rm gal}$ relation extends smoothly from SBHs to nuclei as one moves down the mass function for early-type galaxies (Ferrarese et al. 2006b; see also Wehner & Harris 2006). This suggests that a single mechanism, perhaps star formation or

SBH accretion caused by gas inflows, may be responsible for the growth and/or formation of both types of objects (Ferrarese et al. 2006b). It also suggest that galaxy mass may be the primary (though not necessarily only) parameter regulating such growth. The ACSFCS data will be used to determine the extent to which galaxies in Fornax obey these new scaling relations, and to examine the "universality" of the relations defined by the sample of Virgo galaxies.

2.3. *New Families of Hot Stellar Systems*

Recent years have seen the discovery of stellar systems occupying regions of star cluster parameter space that had not been well explored before. One such class of objects are the so-called ultra-compact dwarfs (UCDs; Hilker et al. 1999; Drinkwater et al. 2000), apparently old stellar systems that are characterized by masses $M \gtrsim 5 \times 10^6 M_\odot$ and sizes $r_e \lesssim 50$ pc (see Haşegan et al. 2005 and references therein, where the term Dwarf-Globular Transition Objects [DGTOs] was introduced to avoid biasing the classification of these unusual objects as either dwarf galaxies or star clusters). In Virgo we found that some of the DGTOs show rather large sizes as compared to GCs, $r_h \sim 20$ pc, and V-band mass-to-light ratios in the range 6–9 (in solar units), while some objects show properties which are consistent with those of bright GCs (Haşegan et al. 2005). Thus, DGTOs seem to be a mixture of GCs and bona-fide UCDs that show evidence for high mass-to-light ratios.

Another type of stellar system, characterized by their diffuse nature and thus termed Diffuse Star Clusters (DSCs; Peng et al. 2006b), were uncovered in significant numbers in the course of the ACSVCS. They have g-band surface brightness $\mu_g \gtrsim 20$ mag arcsec^{-2}. These star clusters include the "faint fuzzy" clusters found in nearby lenticular galaxies by Brodie & Larsen (2002). At least 12 galaxies in Virgo contained a significant population of DSCs; nine of these galaxies are classified as S0s. The ACSFCS will make it possible to carry out systematic searches for DGTOs and DSCs in a second galaxy cluster, allowing a further characterization of their properties and perhaps providing new clues as to the role of environment in their formation and evolution.

2.4. *The 3-D Structure of Galaxy Clusters and an Improved Calibration of the SBF Distance Method*

Accurate distances for individual galaxies greatly enhance the power of a survey such as the ACSVCS or ACSFCS not only because it is then possible to measure quantities in absolute units rather than relative ones, but also because the study of the three dimensional structure of the cluster has strong implications for models of structure formation. The method of surface brightness fluctuations (SBF; Tonry & Schneider 1988) — in which distances are derived from the ratio of the second and first moments of their stellar luminosity functions — offers an efficient and accurate means of measuring such distances. As with the ACSVCS, the SBF method will be used to derive distances for the ACSFCS program galaxies and to use HST/ACS to provide a new and improved calibration of the SBF technique.

In Mei et al. (2005ab) we have described the data reduction procedures appropriate for SBF measurements with the ACS. Those papers demonstrated the feasibility of these measurements — a non-trivial issue due to the strong geometric distortion of the ACS which requires drizzling the data to an undistorted frame. The interpolations necessary in the last step can affect the power-spectrum of the fluctuations, something that will depend on the kernel used for the drizzling. But as shown in Mei et al. (2005a), the measurements are feasible in spite of this complication.

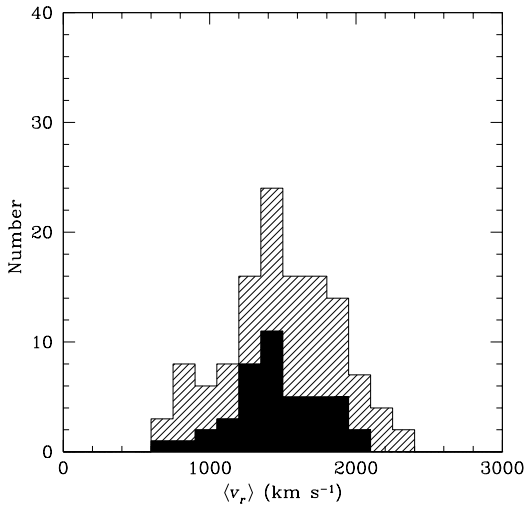

FIG. 2.— Histogram of radial velocities for 125 galaxies of all morphological types identified as likely Fornax cluster members by Ferguson (1989a) and having measured radial velocities according to the NASA Extragalactic Database (*hatched histogram*). The filled histogram shows the radial velocity distribution of the program galaxies of the ACS Fornax Cluster Survey.

However, in order to measure absolute distances with the SBF method, a calibration of the dependence of the fluctuation magnitude on the stellar population content of the galaxy (typically parametrized as an integrated color) is needed. In Mei et al. (2005b), we presented a calibration of the SBF method for the g_{475} and z_{850} bandpasses chosen for the survey and used the resulting distances to examine Virgo's three dimensional structure (Mei et al. 2007).

The Fornax cluster certainly shows some substructure that will be interesting to examine with new and better distances (e.g., Drinkwater et al. 2001a; Dunn & Jerjen 2006). Relative to Virgo, however, the amount of substructure is quite modest. This feature of Fornax, along with its more compact nature, makes it an obvious target for a program to calibrate the SBF relation (with the added benefit that well-calibrated I-band SBF distances exist for 26 Fornax galaxies; Tonry et al. 2001).

3. SAMPLE SELECTION

Target galaxies were selected from the Fornax Cluster Catalog (FCC; Ferguson 1989a), which is based on wide-field blue plates from the 2.5m du Pont telescope at Las Campanas Observatory and digitized plates from the ESO/SRC survey of the southern sky. The Ferguson (1989a) survey, which remains the most complete and homogeneous available for Fornax, covers an area of ~ 40 deg^2 centered at $\alpha \sim 3^h35^m$ and $\delta \sim -35.7°$. Within the survey area, the catalog contains 340 likely cluster members. Memberships were established mainly through

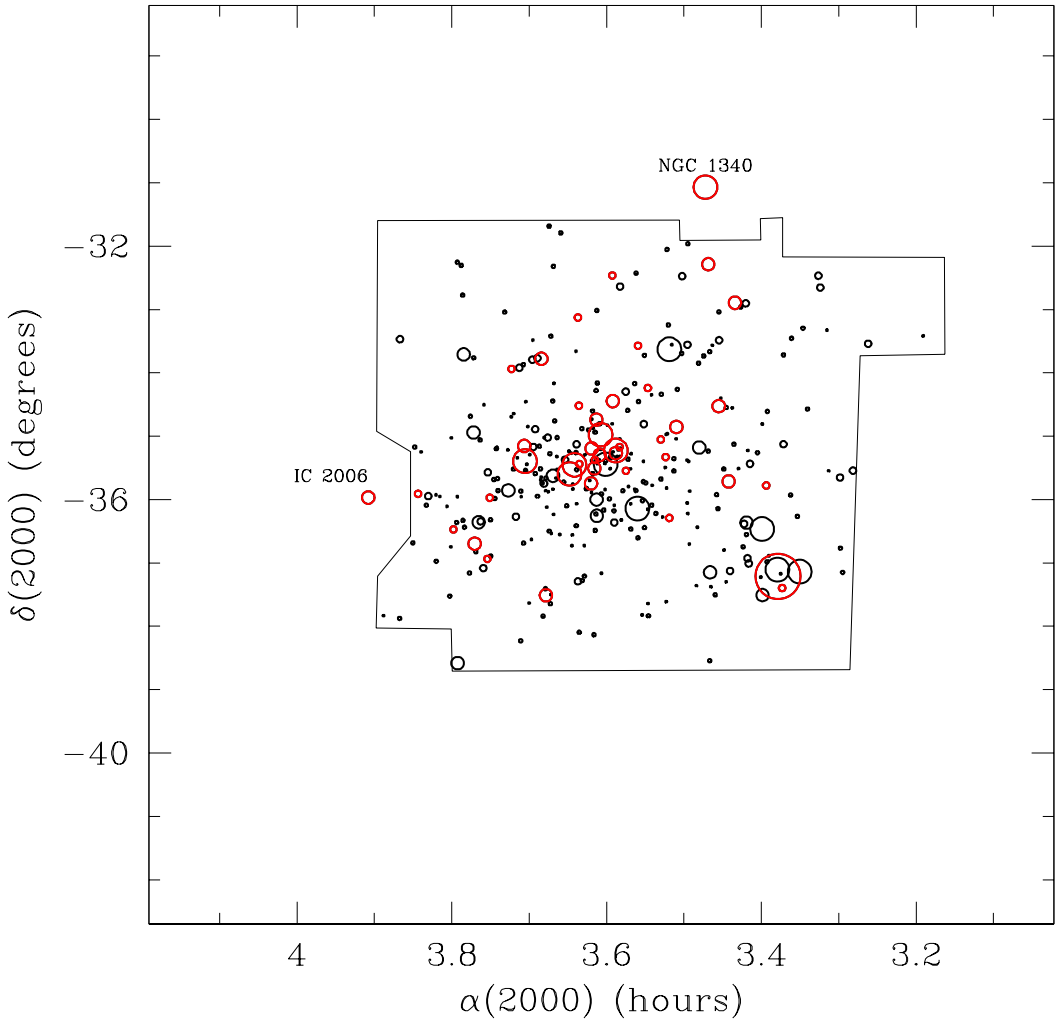

FIG. 3.— Distribution of Fornax Cluster Catalog (FCC) galaxies on the plane of the sky. The outlined region is the area surveyed in constructing the FCC (Ferguson 1989a). The symbol size is proportional to the galaxies' blue luminosity. This figure shows the 340 galaxies within the FCC survey limits that are classified as likely members (i.e., membership codes 1 and 2) of the Fornax cluster, with no restriction on morphological type. Red symbols denote the full sample of 43 early-type galaxies from the ACS Fornax Cluster Survey. Two galaxies that are part of the ACS Fornax Cluster Survey but lie outside of the FCC survey region are labeled (NGC1340 and IC2006). The scale of this figure is the same as Figure 2 in Côté et al. (2004).

galaxy morphology, luminosity and surface brightness, supplemented where possible by a small set of radial velocities.

Among the 340 likely members of Fornax, 79 galaxies have $B_T \leq 15.5$, which is the adopted faint-end cutoff of the ACSFCS. Early-type galaxies were selected from this subset using the FCC morphological classifications. Specifically, program galaxies were required to have morphological types E, S0, SB0, dE, dE,N, dS0, or dS0,N[13]. This selection leaves a total of 44 galaxies. Additionally, we further checked that the galaxies were not classified as late-types in NED; this step eliminated FCC 338 which is classified as type "Sab: sp" in NED. Because one of the main scientific goals of the ACSFCS is an accurate calibration of the z-band SBF distance indicator, two Fornax galaxies that lie outside the FCC survey area were added to the sample (NGC 1340[14] and IC 2006). As a total of 44 orbits were awarded by the TAC, it was necessary to drop one more galaxy in order to accommodate these two additions; as a result, FCC 135 was excluded as it listed by NED as the fainter of the galaxies that have $B_T = 15.5$ according to the FCC.

Unfortunately, the final planned observation of the survey — that of FCC 161 = NGC 1379 — was not completed due to a failure of the telescope to acquire the necessary guide stars and the shutter to open. Thus, the final ACSFCS sample consists of an essentially complete sample of 41 early-type Fornax cluster galaxies brighter than $B_T \sim 15.5$ ($M_B \sim -16$) mag, plus the outlying elliptical galaxies NGC 1340 and IC 2006.

[13] Including two S0/a transition type galaxies: FCC167 and FCC152.

[14] NGC1340 also appears as NGC1344 in the New General Catalogue (of Nebulae and Clusters).

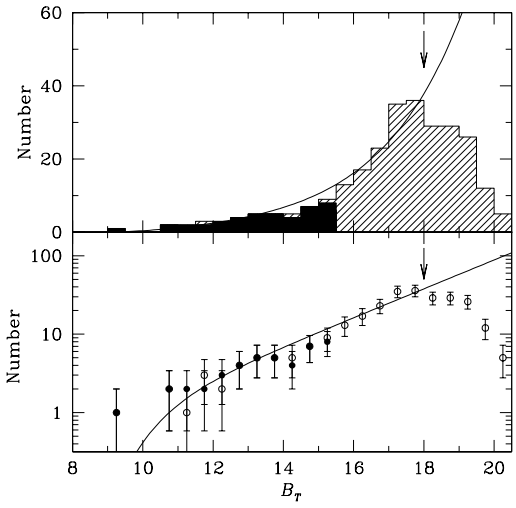

FIG. 4.— (*Upper panel*) Luminosity function of 269 early-type galaxies that are classified by Ferguson (1989a) as members of the Fornax cluster (*upper, hatched histogram*). The arrow shows the FCC completeness limit, while the solid curve shows the best-fit Schechter function for E+S0+dE+dS0 galaxies from Ferguson & Sandage (1991). The filled lower histogram shows the luminosity function for the 43 early-type galaxies in the ACS Fornax Cluster Survey. (*Lower panel*) Same as above, except in logarithmic form. The open circles show the luminosity function of 269 early-type members of the Fornax cluster according to Ferguson (1989a). The arrow shows the completeness limit of the FCC, while the filled circles show the luminosity function of galaxies in the ACS Fornax Cluster Survey. The solid curve is the same as that shown in the upper panel.

According to NED, radial velocities are now available for 125 of the 340 FCC galaxies classified as likely Fornax members by Ferguson (1989a). The hatched histogram of Figure 2 shows the distribution of these 125 galaxies, while the filled histogram shows the distribution of radial velocities for the sample of 43 ACSFCS galaxies. A Kolmogorov-Smirnov test shows that both distributions are consistent with being drawn from the same parent distribution (p-value = 0.91) so we conclude that the velocity distribution for the ACSFCS program galaxies is representative of the full sample of FCC galaxies with available radial velocities.

Figure 3 shows the distribution of the FCC 340 likely Fornax members on the sky (black circles). For comparison, the red circles show the 43 galaxies from the ACSFCS. The scale of this Figure is the same as Figure 2 of Côté et al. (2004), which shows similar data for the Virgo cluster. A comparison of these two figures clearly illustrates the more compact and regular nature of Fornax.

The upper panel of Figure 4 shows the luminosity function of 269 early-type galaxies judged by Ferguson (1989a) to be members of Fornax; the lower panel of this figure shows the same luminosity function in logarithmic form[15]. The filled histogram (*upper panel*) and filled circles (*lower panel*) show the corresponding luminosity functions for the ACSFCS program galaxies, which have $9.4 \leq B_T \leq 15.5$, corresponding to a factor of ≈ 275 in blue luminosity. Note that these galaxies are all considerably brighter than the FCC completeness limit of $B_T \approx 18$ (indicated by the arrows in both panels).

The general properties of the sample galaxies are presented in Table 2. From left to right, the columns of this table record the magnitude ranking from 1 to 43 (which also serves as the identification number for each galaxy in the survey), the FCC, NGC or IC identifier, right ascension and declination, total blue magnitude B_T from Ferguson (1989a), radial velocity, morphological type from the FCC, alternative names in the NGC or ESO catalogs, and references for the radial velocity.[16]

4. OBSERVATIONS

Observations for each of the 43 program galaxies were carried out as part of GO program 10217 between September 2004 and March 2005. Each galaxy was imaged within a single orbit, using the ACS Wide Field Channel (WFC) mode (Ford et al. 1998; Sirianni et al. 2005). This camera consists of two butted 2048×4096 CCD detectors (15μm pixels) having spectral response in the range 0.35–1.05μm. The center of each galaxy was positioned near the WFC aperture, at pixel position (2096, 200) on the WFC1 detector, and then offset perpendicular to the gap between the WFC1 and WFC2 detectors. For the 5 brightest galaxies, this offset was 10″. An offset of 5″ was applied to the remaining galaxies. After correcting for geometrical distortion (see §5), our images have a size of 4256×4256 pixels, with a pixel scale of 0.″049. Thin wedges along the sides of the final image and the $\approx 2.''5$ gap separating the WF1 and WF2 chips are not illuminated, the wedges because of geometric distortion. The resulting field of view is approximately $202'' \times 202''$ in the shape of a rhomboid.

For each galaxy, five images were taken using an identical observing sequence: *i.e.*, two 380 sec exposures in the F475W filter (760 sec total integration in F475W), two 565 sec exposures in the F850LP filter, and a single 90 sec exposure in F850LP (1220 sec total integration in F850LP). The choice of filters was dictated by the long baseline, which results in good sensitivity to metallicity and age of stellar populations, and by the fact that the z-band has good characteristics for SBF measurements; the rationale for the choice of filters is thoroughly documented in §4.1 of Côté et al. (2004). In order to remove chip defects and bad pixels a line dither with a spacing of 0.″146 was performed in the pair of identical exposures of each filter. For some of the program galaxies, the central surface brightness in the redder bandpass can approach $\mu_z(\mathrm{AB}) \simeq 12$ mag arcsec^{-2}, so the 90 sec F850LP exposure was required to repair saturated inner regions in the deeper images. The entire dataset for each galaxy therefore consists of an identical set of images which were reduced and analyzed as described below (§ 5). Except for the slightly larger exposure times and the choice of a line dither pattern, the observational setting is the same as that of the ACS Virgo Cluster Survey.

Table 3 gives the observing log for all ACS observations related to program GO-10217. From left to right, the columns of this table record the identification number of each program galaxy, the Fornax Cluster Catalog number from Ferguson (1989a) (or NGC and IC identifiers), the

[15] For the luminosity function of early-types in Fornax at fainter galaxy magnitudes than those observed by Ferguson (1989a) see Mieske et al. 2006c

[16] Magnitudes and morphological types for IC 2006 and NGC 1340 are taken from NED.

TABLE 2
Basic Data for ACS Fornax Cluster Survey Galaxies.

ID	Name	α (J2000)	δ (J2000)	B_T (mag)	v_r (km s^{-1})	Type	Other	ref
(1)	(2)	(3)	(4)	(5)	(6)	(7)	(8)	(9)
1	FCC 21	03 22 42.09	-37 12 31.63	9.4	1760 ± 10	S0 (pec)	NGC1316	1
2	FCC 213	03 38 29.14	-35 27 02.30	10.6	1425 ± 4	E0	NGC1399	2
3	FCC 219	03 38 52.08	-35 35 37.67	10.9	1947 ± 4	E2	NGC1404	2
4	NGC 1340	03 28 19.7	-31 04 05	11.3	1169 ± 15	E5	NGC1344	3
5	FCC 167	03 36 27.45	-34 58 31.09	11.3	1877 ± 12	S0/a	NGC1380	4
6	FCC 276	03 42 19.16	-35 23 36.03	11.8	1388 ± 3	E4	NGC1427	2
7	FCC 147	03 35 16.74	-35 13 33.94	11.9	1294 ± 2	E0	NGC1374	2
8	IC 2006	03 54 28.45	-35 58 01.7	12.2	1382 ± 3	E	ESO359-G07	5
9	FCC 83	03 30 35.04	-34 51 14.51	12.3	1514 ± 3	E5	NGC1351	5
10	FCC 184	03 36 56.84	-35 30 23.85	12.3	1302 ± 12	SB0	NGC1387	6
11	FCC 63	03 28 06.55	-32 17 05.87	12.7	1392 ± 3	E4	NGC1339	2
12	FCC 193	03 37 11.67	-35 44 39.73	12.8	921 ± 12	SB0 (5)	NGC1389	7
13	FCC 170	03 36 31.59	-35 17 43.35	13.0	1724 ± 9	S0(9)(boxy)	NGC1381	4
14	FCC 153	03 35 30.91	-34 26 44.74	13.0	1619 ± 6	S0 (9)	ESO358-G26	4
15	FCC 177	03 36 47.35	-34 44 17.25	13.2	1561 ± 6	S0 (9)(cross)	NGC1380A	4
16	FCC 47	03 26 31.97	-35 42 44.59	13.3	1418 ± 3	E4	NGC1336	2
17	FCC 43	03 26 02.30	-32 53 36.80	13.5	1323 ± 17	dS0 /2 (5),N	ESO358-G01	7
18	FCC 190	03 37 08.86	-35 11 37.54	13.5	1740 ± 17	SB0	NGC1380B	7
19	FCC 310	03 46 13.67	-36 41 43.24	13.5	1373 ± 13	SB0	NGC1460	7
20	FCC 249	03 40 41.92	-37 30 33.30	13.6	1613 ± 34	E0	NGC1419	8
21	FCC 148	03 35 16.79	-35 15 55.95	13.6	740 ± 6	S0(cross)	NGC1375	4
22	FCC 255	03 41 03.40	-33 46 38.42	13.7	1255 ± 23	S0 (6),N	ESO358-G50	3
23	FCC 277	03 42 22.60	-35 09 10.22	13.8	1640 ± 8	E5(boxy)	NGC1428	2
24	FCC 55	03 27 17.90	-34 31 29.17	13.9	1279 ± 17	S0(9),N	ESO358-G06	7
25	FCC 152	03 35 33.09	-32 27 44.79	14.1	1389 ± 12	S0/a pec	ESO358-G25	7
26	FCC 301	03 45 03.49	-35 58 16.95	14.2	1007 ± 18	E4	ESO358-G59	3
27	FCC 335	03 50 36.64	-35 54 29.27	14.2	1430 ± 2	E	ESO359-G02	2
28	FCC 143	03 34 59.06	-35 10 09.90	14.3	1334 ± 2	E3	NGC1373	2
29	FCC 95	03 31 24.68	-35 19 46.41	14.6	1275 ± 26	dSB0 or dSBa		7
30	FCC 136	03 34 29.39	-35 32 41.18	14.8	1205 ± 1	dE2,N		2
31	FCC 182	03 36 54.24	-35 22 22.69	14.9	1657 ± 19	SB0 pec		7
32	FCC 204	03 38 13.60	-33 07 31.29	14.9	1369 ± 28	dS0(8),N	ESO358-G43	7
33	FCC 119	03 33 33.73	-33 34 17.84	15.0	1374 ± 7	S0 pec		2
34	FCC 90	03 31 08.06	-36 17 19.48	15.0	1813 ± 15	E4 pec		7
35	FCC 26	03 23 37.16	-35 46 38.68	15.0	1823 ± 29	SB0 (8)	ESO357-G25	3
36	FCC 106	03 32 47.62	-34 14 14.18	15.1	2064 ± 35	d:S0(6),N		7
37	FCC 19	03 22 22.77	-37 23 45.55	15.2	1497 ± 47	dS0 (8),N	ESO301-G08	7
38	FCC 202	03 38 06.40	-35 26 17.96	15.3	808 ± 22	d:E6,N	NGC1396	7
39	FCC 324	03 47 52.61	-36 28 13.25	15.3	1856 ± 29	dS0 (8)	ESO358-G66	3
40	FCC 288	03 43 22.61	-33 56 14.78	15.4	1189 ± 29	dS0(9),N	ESO358-G56	3
41	FCC 303	03 45 13.93	-36 56 07.63	15.5	1980 ± 31	dE1,N		7
42	FCC 203	03 38 09.10	-34 31 01.08	15.5	1138 ± 28	dE6,N	ESO358-G42	7
43	FCC 100	03 31 47.52	-35 03 00.72	15.5	1660 ± 31	dE4,N		7

Note. — Key to columns—(1) Galaxy ID; (2) FCC, NGC or IC identifier; (3)-(4) Right ascension and declination; (5) Total B_T magnitude from Ferguson (1989a); (6) Radial velocity from the reference indicated in the last column and obtained via NED; (7) Morphological classification from Ferguson (1989a); (8) Alternative NGC or ESO identifier when available; (9) Reference for radial velocity: 1.- Longhetti et al. (1998); 2.- Graham et al. (1998); 3.- de Vaucouleurs et al. (1995) (RC3); 4.- D'Onofrio et al. (1995); 5.- Smith et al. (2000); 6.- Menzies, Coulson & Sargent (1989) ; 7.- Drinkwater et al. 2001b; 8.- da Costa et al. (1998).

universal date of the observation, the dataset name, the universal time at the start of each observation and the position angle, Θ, of the y axis of the WFC1 detector. The final two columns give the exposure time and filter for each observation. NGC and ESO identifiers for those galaxies that have them may be found in Table 2.

5. DATA REDUCTION PROCEDURES

5.1. *Image Reductions*

The ACSFCS data reduction procedures are nearly identical to the ones adopted for the ACSVCS. The customized data reduction pipeline developed to reduce the ACSVCS data has been documented in detail in Jordán et al. (2004b; hereafter J04). Wherever possible we retained the identical procedures for the two surveys to ensure the maximum level of homogeneity. In what follows, we briefly summarize the main steps in the reduction process and describe in detail only those aspects of the ACSFCS analysis that differ from the ones outlined in J04.

The data reduction pipeline consists of a series of steps which are summarized graphically in Figure 1 of J04. In the first of these, the raw images are registered using a source matching algorithm (see §2.2 of J04) and the empirically measured shifts are then used with *multidrizzle* (Koekemoer et al. 2002) to create geometrically corrected, cosmic-ray cleaned images of dimension 4256 × 4256 pixel (see §§2.2, 2.3 in J04). Measuring accurate shifts between the images is important to obtain the highest quality combined images (White 2006).

In contrast to the ACSVCS, the analysis for the ACSFCS will rely exclusively on images drizzled with a

TABLE 3
Log of Observations for GO-10217.

ID	Name	Date	Dataset	UT	Θ (deg)	T (sec)	Filter
1	FCC 21	2005 Feb 16	j90x01i7q	03:09:30	85.95	90	F850LP
			j90x01i8q	03:13:18	85.95	565	F850LP
			j90x01iaq	03:25:19	85.95	565	F850LP
			j90x01icq	03:37:57	85.95	380	F475W
			j90x01ieq	03:46:53	85.95	380	F475W
2	FCC 213	2004 Sep 11	j90x02e6q	07:59:03	281.46	90	F850LP
			j90x02e7q	08:02:51	281.46	565	F850LP
			j90x02e9q	08:14:52	281.46	565	F850LP
			j90x02ebq	08:27:30	281.46	380	F475W
			j90x02edq	08:36:26	281.46	380	F475W

[a]Table 3 is presented in its entirety in the electronic version of this paper. A portion is shown here for guidance regarding its form and content.

"Lanczos3" kernel, as this kernel gives a sharper PSF in the drizzled image. Given the unexpected but frequent occurence of marginally-resolved stellar nuclei in the ACSVCS galaxies (Côté et al. 2006; Ferrarese et al. 2006ab), this improvement in resolution for the slightly more distant Fornax sample is deemed more important than the superior ability of the "Gaussian" kernel to repair defective pixels (which was used in the ACSVCS for the isophotal analysis). The value of the "bits" parameter, which indicates which pixels are to be considered good based on their value in the data quality file and thus drizzled into the final image, was determined according to the date the data were taken, as there was a change in the convention that defines the bits value: for observations taken before October 1, 2004 we adopted `bits` = 14594 and `bits` = 14658 for all subsequent observations.

Weight images were constructed in order to perform object detection and to aid in the determination of photometric and structural parameters of GCs. Weight images were constructed as described in §2.4 of J04 except that a different contribution from SBF to the "noise" was adopted in order to account for the higher mean distance to the Fornax cluster compared to Virgo. This SBF "noise" is added to avoid detection of spurious sources corresponding to real fluctuations, in particular in the z-band. Following the notation of J04, the contribution of SBF to the weight images W'_{ij} was given by κO_{ij} with $\kappa = 0.073$ and 2.19 for the g- and z-band respectively. These values were derived by assuming that Fornax is a factor of 1.17 more distant than the Virgo cluster (Tonry et al. 2001).

Internal dust obscuration in some galaxies, usually in the central regions, significantly affects the surface brightness profiles. This poses problems for both object detection and estimation of the local background over which sources are detected. We used the method described in §2.4 of J04, and discussed in more detail in Ferrarese et al. (2006a), to mask pixels affected by dust when necessary. Pixels found to be affected by dust are then given zero weight in the weight images. The galaxies that needed masking because of dust obscuration are FCC 21, FCC 119, FCC 152, FCC 167, FCC 184, FCC 219, FCC 335 and FCC 90.

A two-dimensional galaxy model for each program galaxy was then constructed in order to determine the weight maps and, more importantly, to subtract the galaxy light and perform object detection on a nearly flat background. As in the ACSVCS (see §2.5 in J04) most galaxies were modeled using the ELLIPROF program described in the SBF survey of Tonry et al. (1997), masking regions affected by dust when necessary.

However, for three of the galaxies, ELLIPROF was unable to produce acceptable models because of the presence of strong edge-on disk components that were not well approximated by elliptical isophotes modulated by low-order Fourier terms[17]. In these cases, we masked the disk with a rectangular region and then modeled the galaxy outside this region by using the multi-gaussian expansion algorithm of Cappellari (2002) for FCC 153 and FCC 177 and by using SExtractor to fit a two-dimensional bicubic spline for FCC 170. The masked regions are considered no further in the analysis of the star clusters.

An important step in constructing the galaxy models is the determination of the background "sky" rates, $f_{\rm back}$, for each galaxy. Figure 5 shows the measured count rates in F475W and F850LP, in units of electrons pixel^{-1} s^{-1}, for the full sample of galaxies. These count rates are obtained by estimating the mode at distances $\approx 90''$–$120''$ from the galaxy center. The upturn seen for a few of the brighter galaxies is due to the fact that the galaxy itself fills the field of view, thereby biasing the background estimation.

In the ACSVCS, it was found that the local background scaled with the angle $\Phi_{\rm Sun}$ between the Sun and the V1 axis of the telescope. That lead us to fit a function of the form $f_{\rm back} = a_i \exp^{b_i(\Phi_{\rm Sun}-c_i)} + d_i$ to the 90 faintest VCS galaxies and then use the best fit values of the parameters a_i, b_i, c_i and d_i to predict $f_{\rm back}$ for the bright galaxies with biased background estimates. In the case of the ACSFCS, there is no obvious dependence of the background level on $\Phi_{\rm Sun}$, as illustrated in Figure 6. Therefore, to estimate the background for the five brighter galaxies in the sample we adopted constant background levels of 0.03324 and 0.02159 electrons pixel^{-1} s^{-1} for F475W and F850LP, respectively. These values are indicated by the dashed lines in Figure 6. The dot-dashed curves show the models adopted in the ACSVCS, illustrating that the background levels are lower for galaxies

[17] These galaxies are FCC 153, FCC 170 and FCC 177.

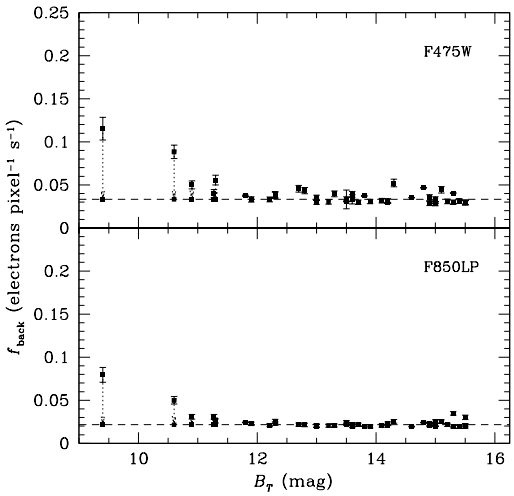

FIG. 5.— Background count rates measured at $R \gtrsim 90''$ in the F475W and F850LP images(upper and lower panels, respectively). Apart from the brightest galaxies, the background levels are well represented by the values $f_{\rm back} = 0.03324$ and $f_{\rm back} = 0.02159$ electrons pixel^{-1} s^{-1} in the F475W and F850LP bands, respectively. These values are indicated by the dashed lines in each panel.

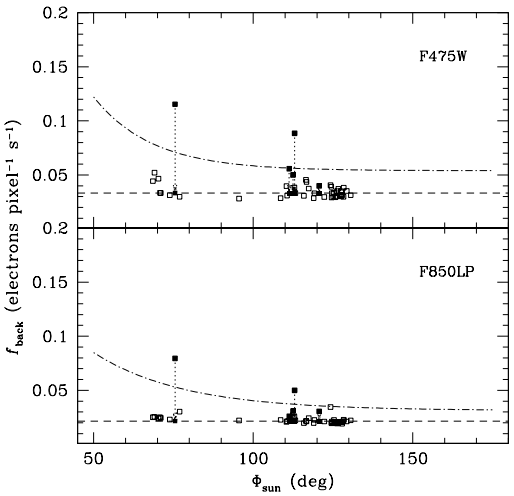

FIG. 6.— Background count rates in F475W (upper panel) and F850LP (lower panel) plotted as a function of $\Phi_{\rm Sun}$. The sky levels show no clear dependence on $\Phi_{\rm Sun}$. The dashed lines in the two panels show sky levels of 0.03324 and 0.02159 electrons pixel^{-1} s^{-1} in F475W and F850LP, respectively. These values were used to estimate the background for the five brighter galaxies in the sample. The dot-dashed curve show a parametric representation of the form of eq. (5) in Jordán et al. (2004) which was the adopted form for the background rates as a function of $\Phi_{\rm Sun}$ for the ACS Virgo Cluster Survey. The measured count rates for the five brightest galaxies are shown by the upper filled squares; the adopted values are indicated by the lower filled squares.

in Fornax[18]. The difference in the level and behavior of the background levels is likely due to the low ecliptic latitude of Virgo ($\beta \approx 14.4°$) as compared to that of Fornax ($\beta \approx -52.8°$).

Objects were detected by running SExtractor (Bertin & Arnouts 1996) on images in which the background (including the galaxy light) was subtracted using the procedures detailed in §2.5 of J04. Sources were detected independently in the two bands and then matched using a matching radius of $0\farcs1$. Beginning with the complete list of detections, a first selection on magnitude and elongation is then made to isolate potential GC candidates for further analysis, as described in §2.6 of J04. The only difference in this procedure in the case of the ACS-FCS is that, when selecting in magnitude, we assume that the peak of the GC luminosity function is 0.34 mag fainter due to the larger relative distance of Fornax (i.e., $d_{\rm fornax}/d_{\rm virgo} = 1.17$; Tonry et al. 2001).

All sources flagged as potential GCs are then run through a code (KINGPHOT) that fits a PSF-convolved King (1966) model to the observed light distribution of each object (Jordán et al. 2005). This provides measurements of both the King structural parameters for the sources as well as their total magnitudes. Performing such measurements requires accurate models for the PSFs, something that proved challenging in the ACS-FCS. These challenges, and the adopted solutions, are described in detail below (§5.2).

The pixel coordinates of the detections were first converted to celestial coordinates using the header information. We then compared the coordinates of 371 astrometric standards within our survey fields to those listed in the Guide Star Catalog 2.3 (McLean et al. 1998). For 35 galaxies which had enough objects to derive a reliable correction, we applied offsets in right ascension and declination to the celestial coordinates derived from the headers. The mean corrections were $-0\farcs016$ in right ascension and $0\farcs34$ in declination. The internal accuracy of the celestial coordinates for a given galaxy is $\approx 0\farcs01$ (Meurer et al. 2002).

A reddening for each galaxy was computed using the DIRBE maps of Schlegel, Finkbeiner & Davis (1998). The mean reddening for the whole sample was found to be $\langle E(B-V)\rangle = 0.013$ mag with a dispersion around this value of $\sigma_{E(B-V)} = 0.003$ mag. The extinction ratios and photometric zeropoints adopted are those described in §2.7 of J04 (which were derived using information from Sirianni et al. 2005).

A consequence of the environment of HST on silicon-based CCDs is to decrease their charge transfer efficiency (CTE) with time, especially along the serial direction (e.g., Riess & Mack 2004). CTE degradation has the effect of reducing the apparent flux of objects, which in turn potentially requires corrections to the photometry in order to recover the "true" flux of objects. We have used the CTE corrections for ACS/WFC presented in Riess & Mack (2004) to estimate the effect of CTE degradation on our survey. The worst case scenario is offered by a source at the detection limit in g_{475} (26.35), observed at the latest date our data were taken and subject to 2048 serial pixel transfers. In this case we expect charge transfer inefficiency to dim the source by ≈ 0.025 mag. A typical source with $g_{475} = 24$, observed at the average date for our survey and subject to 1024 serial pixel transfers would be dimmed by ≈ 0.004 mag. Given the modest magnitude of the flux loss in the worst case scenario and the small effect of CTE degradation for a typical source we choose not to apply CTE correction to

[18] Of the four faint ACSFCS galaxies that show higher backgrounds in F475W two (including the one showing the highest background) have luminous companions within $\sim 5'$: FCC 143 is projected close to FCC 147 and FCC 202 to FCC 213=NGC 1399.

our photometry.

The final step in generating GC catalogs is the selection of candidate GCs from the set of objects/detections that passed the initial selection criteria on magnitude and elongation. This selection is done using a mixture model algorithm that separates probable GCs from contaminants, assigning to each source a probability $p_{\rm GC}$ that it is indeed a GC. This selection procedure is described in detail in Jordán et al. (2007, in preparation). This paper also includes a discussion of the methods by which the aperture corrections are determined for the GCs.

5.2. *Point Spread Function and Globular Cluster Size Measurements*

After an initial run of KINGPHOT on the detected GC candidates, it was noticed that, in some galaxies, the mean half-light radii $\langle r_{h,g}\rangle$ in the g-band was significantly larger than the corresponding value $\langle r_{h,z}\rangle$ in the z-band. In the ACSVCS, differences in $\langle r_h\rangle$ between the two bands satisfied $|\langle r_{h,g} - r_{h,z}\rangle| \lesssim 0.1$ pixel (see Jordán et al. 2005). However, for some ACSFCS galaxies this difference was significantly larger: up to ≈ 0.5 pixels in a few cases (see Figure 7). As the underlying objects are the same, the sizes in the two bandpasses should be roughly equal in the average.

Given that a study of the GC size distribution function and a comparison with the Virgo results presented in Jordán et al. (2005) is one of the main goals of the ACSFCS, it was necessary to determine the root cause of this problem and/or to provide a means for correcting it. Aside from the obvious challenge that this problem might impose on the interpretation of the size distribution function, it could lead to unacceptably large (and systematic) differences in the GC magnitudes derived from the fitted models.

As a first attempt to solve the problem, a new set of PSFs was constructed using $\gtrsim 1000$ stars in fields located in the outskirts of the Galactic GC 47 Tucanae (programs GO-10048 and GO-10375). We determined three different PSFs using observations taken in September 2004, December 2004 and February 2005. By doing so, we generated an empirical PSF for each galaxy that was determined no more than two months from the ACSFCS observations. This procedure was motivated by the fact that, on 20 December 2004, HST underwent a secondary mirror adjustment (which the observatory is regularly subjected to in order to correct systematic changes in the relative position of the primary and secondary mirrors). In this particular case, the secondary mirror was moved by 4.16μm, a sizable displacement which certainly changed the focus and affected the PSF (Krist 2003). Although the empirically derived PSFs clearly reveal the post-movement PSF to show a more compact core, a redetermination of the GC sizes showed that these new PSFs did not solve the anomalous sizes found in the g-band. Nevertheless, the new PSFs do constitute an improvement over the single PSF approach adopted for the ACSVCS (both in terms of time sampling and number of stars used to construct the PSF) so we kept them for the analysis of all galaxies that do not show an anomalous size difference. For galaxies that were observed after 20 December 2004, we used the PSF determined on February 2005; for the ones observed before, we used the closest in time of the other two PSFs.

While the cause of the problem was under investigation, Anderson & King (2006) published a comprehensive study of the WFC PSF, including an analysis of its time variability. They find that the WFC PSF varies on orbital timescales in an unpredictable way, with variations in the core flux of up to $\sim 10\%$. Moreover, these variations are more pronounced in the bluer filters as compared to a red one (see their Figure 8). This closely resembles the behavior that is seen in the ACSFCS data — core flux variations of that order in the g-band would easily result in the derived r_h being systematically higher by tenths of a pixel while being insignificant in the near-infrared z-band. The rapid time variability of the effect is clearly illustrated by the pair of giant elliptical galaxies FCC 213 and FCC 219. Both galaxies contain sizable GC populations and thus have excellent statistics on the average size difference between the two bands. Yet, despite the fact that the observations were carried out within a day of each other, FCC 213 showed a difference of ~ 0.15 pixel while that for FCC 219 was essentially zero.

The results of Anderson & King (2006) suggest that the only viable way to correct the wider PSF in the g-band is to identify on-frame stellar objects and use them to empirically correct the PSFs that were constructed from the 47 Tucanae fields. Of course, the drawback of this procedure is that the accuracy of any such correction will be limited by the number of suitable stars that can be found. We proceeded by first identifying all galaxies that required a correction. To do this, the measured r_h in both bands were used to compute $\langle r_{h,g} - r_{h,z}\rangle$ for a sample of objects satisfying $z_{850} < 23.5$ mag and $0\farcs01 < \langle r_h\rangle < 0\farcs05$ — criteria that ensure the sample is dominated by GCs (Jordán et al. 2005). We then flagged those galaxies for which

$$\langle r_{h,g} - r_{h,z}\rangle > \max(0.1\,{\rm pix}, 4\sigma) \qquad (1)$$

where σ is the standard deviation of the mean. A total of seven galaxies were identified in this way: FCC 213, IC 2006, FCC 193, FCC 249, FCC 277, FCC 19 and FCC 202.

For these galaxies, we adopted the following approach to correct the PSFs. First, in each case, we identified from the SExtractor catalog of the z-band image a set of probable stars by selecting objects with CLASS_STAR > 0.8, full-width at half-maximum FHWM < 2.5 pixel and z-magnitude in a 4-pixel aperture $z_{\rm ap} < 20$ mag. These objects were then inspected visually to verify the automated selection; this step resulted in the rejection of a single star candidate in just one galaxy (FCC 19). The number of stars found in each galaxy ranged from 5 to 8. Once these stars were selected, we determined for each of the affected galaxies a perturbation to the g-band PSF to adjust it to the selected on-frame stars. That is to say, if we denote the normal survey PSF by $\mathcal{P}_{ij}$, and the PSF that best describes the on-frame stars (in a least squares sense) by $\mathcal{S}_{ij}$, then we determined for each of the g-band observations a perturbation δ_{ij} such that $\mathcal{S}_{ij} = \delta_{ij} + \mathcal{P}_{ij}$. Here δ_{ij} is an array of the average difference between the identified stars and the $\mathcal{P}_{ij}$. For the affected galaxies, sizes in the g-band were then determined using the perturbation δ_{ij} on top of the normal survey PSF. Given that the PSF quality is limited by the small number of stars used to determine each perturbation, the g-band sizes in these galaxies are of

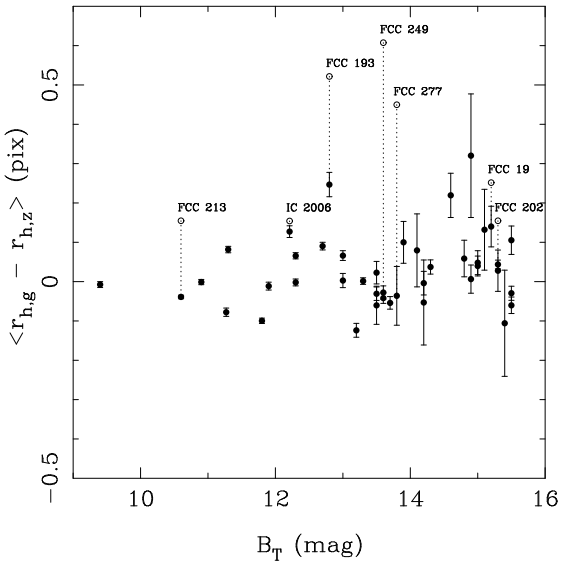

FIG. 7.— Median difference $\langle r_{h,g} - r_{h,z} \rangle$ between the half-light radii r_h measured in the g- and z-bands as a function of total galaxy B_T magnitude (solid points). The mean difference is estimated as described in §5.2. Open symbols denote the galaxies that were flagged as having an anomalously large difference in the mean size and whose GC sizes were re-measured using a corrected PSF built using on-frame stars (see §5.2). The FCC identification numbers of those galaxies is indicated next to the open symbols. The dashed lines connect to the measured r_h difference after the correction was performed.

somewhat lower quality than the corresponding g-band measurements in the remaining 36 galaxies.

The results of the procedure are summarized in Figure 7 which plots $\langle r_{h,g} - r_{h,z} \rangle$ against galaxy magnitude B_T for the 42 galaxies for which we could measure this quantity[19]. Open symbols indicate the initial measurements for those galaxies which were found to satisfy equation (1). The dotted lines connect to solid points that indicate the value of $\langle r_{h,g} - r_{h,z} \rangle$ using the corrected PSF. As seen in the figure, our procedure brings the behavior of $\langle r_{h,g} - r_{h,z} \rangle$ to acceptable levels for most galaxies in the sample. We emphasize that at no point in the process do we *force* $\langle r_{h,g} - r_{h,z} \rangle$ to decrease. The improved agreement results naturally from the perturbation to the PSF calculated using the on-frame stars selected from the z-band observations. After the correction procedure, we proceed with the analysis knowing that the size measurements are consistent, to within $\lesssim 0.1$ pixel, between the two bands for the bulk of the ACSFCS sample.

[19] The galaxy FCC 119 was not left with enough GC candidates after the cuts described above to calculate $\langle r_{h,g} - r_{h,z} \rangle$.

6. SUMMARY

We have provided a brief introduction to the ACS Fornax Cluster Survey (GO-10217), an HST program to image 43 early-type galaxies brighter than $M_B \approx -16$ in the Fornax cluster. In conjunction with a similar survey of 100 early-type galaxies in the Virgo cluster — the ACS Virgo Cluster Survey (Côté et al. 2004) — the final sample of F475W and F850LP imaging for 143 galaxies represents the most comprehensive imaging dataset currently available for early-type galaxies in nearby cluster environments. We have briefly described the observing strategy and the data reduction procedures adopted for the survey. Scientific results from the survey will be presented in future papers in this series. Additional information on the ACS Fornax Cluster Survey can be found at the program website: `http://www.eso.org/ ajordan/ACSFCS/`.

Support for program GO-10217 was provided through a grant from the Space Telescope Science Institute, which is operated by the Association of Universities for Research in Astronomy, Inc., under NASA contract NAS5-26555. P.C. acknowledges additional support provided by NASA LTSA grant NAG5-11714. L.I. acknowledges additional support from FONDAP Center of Astrophysics. This research has made use of the NASA/IPAC Extragalactic Database (NED) which is operated by the Jet Propulsion Laboratory, California Institute of Technology, under contract with the National Aeronautics and Space Administration.

Facility: HST (ACS/WFC)

REFERENCES

Abell, G.O., Corwin, H.G., & Olowin, R.P. 1989, ApJS, 70, 1
Anderson, J., & King, I. 2006, STScI Instrument Science Report ACS 2006-01
Bertin, E. & Arnouts, S. 1996, A&AS, 117, 393
Brodie, J.P., & Larsen, S.S. 2002, AJ, 124, 1410
Baum, W.A. 1955, PASP, 67, 328
Binggeli, B., Sandage, A., & Tammann, G.A., 1985, AJ, 90, 1681
Binggeli, B., Sandage, A., & Tammann, G.A., 1987, AJ, 94, 251
Binggeli, B. 1999, in Ringberg Workshop, The Radio Galaxy Messier 87, ed. H.-J. Rser & K. Meisenheimer (Berlin: Springer), 9
Böker, T., Laine, S., van der Marel, R.P., Sarzi, M., Rix, H.-W., Ho, L., & Shields, J.C. 2002, AJ, 123, 1389
Böker, T., Sarzi, M., McLaughlin, D.E., van der Marel, R.P., Rix, H.-W., Ho, L.C., & Shields, J.C. 2004, AJ, 127, 105
Carollo, C.M., Franx, M., Illingworth, G.D., & Forbes, D.A. 1997, ApJ, 481, 710
Carollo, C.M., Stiavelli, M., & Mack, J. 1998, AJ, 116, 68
Cappellari, M. 2002, MNRAS, 333, 400
Clark, G. W. 1975, ApJ, 199, L143
Côté, P., et al. 2004, ApJS, 153, 223 (ACSVCS Paper I)
Côté, P., et al. 2006, ApJS, 165, 57 (ACSVCS Paper VIII)
Crane, P., et al. 1993, AJ, 106, 1371
Croton, D.J., et al. 2006, MNRAS, 365, 11
da Costa, L., et al. 1998, AJ, 116, 1
de Vaucouleurs, G., de Vaucouleurs, A., Corwin, H. G., Buta, R. J., Paturel, G., & Fouqu, P. 1995, Third Reference Catalogue of Bright Galaxies (Austin: University of Texas Press) (RC3)
Dawe, J.A., & Dickens, R.J. 1975, Nature, 263, 395
D'Onofrio, M., Zaggia, S.R., Longo, G., Caon, N., & Capaccioli, M. 1995, A&A, 296, 319
Drinkwater, M.J., Jones, J.B., Gregg, M.D., & Phillipps, S. 2000, PASA, 17, 227
Drinkwater, M.J., Gregg, M.D., & Colless, M. 2001a, ApJ, 548, L139
Drinkwater, M.J., Gregg, M.D., Holman, B.A., & Brown, M.J.I. 2001b, MNRAS, 326, 1076
Dunn, L.P., & Jerjen, H. 2006, AJ, 132, 1384
Evans, D.S. 1951, Discovery, 12, 315
Fabbiano, G., 2006, ARA&A, 44, 323
Ferguson, H.C. 1989a, AJ, 98, 367
Ferguson, H.C. 1989b, ApSS, 157, 227

Ferguson, H.C., & Sandage, A. 1991, AJ, 101, 765
Ferrarese, L., et al. 1994, AJ, 108, 1598
Ferrarese, L., et al. 1996, ApJ, 464, 568
Ferrarese, L., & Ford, H. 2005, SSRv, 116, 523
Ferrarese, L. et al. 2006a, ApJS, 164, 334 (ACSVCS Paper VI)
Ferrarese, L., et al. 2006b, ApJ, 644, L21
Ford, H.C., et al. 1998, Proc. SPIE, 3356, 234
Freedman, W. L., et al. 1994, Nature, 371, 757
Fukazawa, Y., Makishima, K., Tamura, T., Ezawa, H., Xu, H., Ikebe, Y., Kikuchi, K., & Ohashi, Y. 1997, PASJ, 50, 187
Gavazzi, G., Boselli, A., Donati, A., Franzetti, P., & Scodeggio, M. 2003, A&A, 400, 451
Girardi, M., Biviano, A., Giuricin, G, Mardirossian, F., & Mezzetti, M. 1995. ApJ, 438, 527
Graham, A.W., Colless, M.M., Busarello, G., Zaggia, S., & Longo, G. 1998 A&AS, 133, 325
Graham, A.W., Erwin, P., Trujillo, I., & Asensio Ramos, A. 2003, AJ, 125, 2951
Haşegan et al. 2005, ApJ, 627, 203 (ACSVCS Paper VII)
Hanes, D.A., & Harris, W.E. 1986, ApJ, 309, 564
Harris, W.E. 2001, in Star Clusters, Saas-Fee Advanced School 28, ed. L. Labhardt & B. Binggeli (Berlin:Springer), 223
Hilker, M., Infante, L., Vieira, G., Kissler-Patig, M., & Richtler, T. 1999, A&AS, 134, 75
Hodge, P.W., 1959, PASP, 71, 28
Hodge, P.W., 1960, PASP, 72, 188
Hodge, P.W., Pyper, D.M. & Webb, C.J. 1965, AJ, 70, 559
Huchra, J. 1985, in The Virgo Cluster, ESO Workshop proceedings No. 20, ed. O.-G. Richter & B. Binggeli, ESO, Garching, p. 181
Humason, M.L., Mayall, N.U., & Sandage, A.R. 1956, AJ, 61, 97
Jordán, A. et al. 2004a, ApJ, 613, 279 (ACSVCS Paper III)
Jordán, A. et al. 2004b, ApJS, 154, 509 (ACSVCS Paper II; J04)
Jordán, A. et al. 2005, ApJ, 634, 1002 (ACSVCS Paper X)
Jordán, A. et al. 2006, ApJ, 651, L25.
Jordán, A. et al. 2007, ApJS, submitted (ACSVCS Paper XII)
Katz, J. I. 1975, Nature, 253, 698
King, I.R. 1966, AJ, 71, 64
Koekemoer, A.M., Fruchter, A.S., Hook, R.N., & Hack, W. 2002, in The 2002 HST Calibration Workshop, ed. S. Arribas, A. Koekemoer, & B. Whitmore (STScI: Baltimore), p 339.
Kormendy, J., & Djorgovski, S.G. 1989, ARA&A, 27, 235
Krist, J. 2003, STScI Instrument Science Report ACS 2003-06
Lauer, T.R., et al. 1995, AJ, 110, 2622
Longhetti, M., Rampazzo, R., Bressan, A., & Chiosi, C. 1998, A&AS, 130, 267
Machacek, M., Dosaj, A., Forman, W., Jones, C., Markevitch, M., Vikhlinin, A., Warmflash, A., & Kraft, R. 2005, ApJ, 621, 663
Madore, B.F., et al. 1999, ApJ, 515, 29
Matthews, L.D., et al. 1999, AJ, 118, 208
McLaughlin, D.E. 1999, ApJ, 512. L9
Mei, S., et al. 2005a, ApJS, 156, 113 (ACSVCS Paper IV)
Mei, S., et al. 2005b, ApJ, 625, 121 (ACSVCS Paper V)
Mei, S., et al. 2007, ApJ, 655, 144 (ACSVCS Paper XIII)
Menzies, J.W., Coulson, I.M., & Sargent, W.L.W. 1989, AJ, 97, 1576
McLean, B., Hawkins, C., Spagna, A., Lattanzi, M., Lasker, B., Jenkner, H., White, R. 1998, in IAU Symp. 179, New Horizons from Multi-Wavelength Sky Surveys, ed. B.J. McLean, D.A. Golombek, J.J.E. Hayes, & H.E. Payne (Dordrecht: Kluwer), 431
Meurer, G.R., Lindler, D., Blakeslee, J.P., Cox, C., Martel, A.R., Tran, H.D., Bouwens, R.J., Ford, H.C., Clampin, M., Hartig, G.F., Sirianni, M., & de Marchi, G. 2002, in The 2002 HST Calibration Workshop, ed. S. Arribas, A. Koekemoer, & B. Whitmore (STScI: Baltimore), p 65.
Mieske, S., Hilker, M., Infante, L., & Jordán, A. 2006a, AJ, 131, 2442
Mieske, S., et al. 2006b, ApJ, 653, 193 (ACSVCS Paper XIV)
Mieske, S., Hilker, M., Infante, L, & Mendes de Oliveira, C. 2006c, A&A, in press (`astro-ph/0610516`)
Peng, E.W. et al. 2006a, ApJ, 639, 95 (ACSVCS Paper IX)
Peng, E.W. et al. 2006b, ApJ, 639, 838 (ACSVCS Paper XI)
Reaves, G., 1956, AJ, 61, 69
Riess, A., & Mack, J. 2004, STScI Instrument Science Report ACS, 2004-006
Rossa, J., van der Marel, R.P., Böker, T., Gerssen, J., Ho, L.C., Rix, H.-W., Shields, J.C., & Walcher, C.-J. 2006, AJ, 132, 1074
Scharf, C.A., Zurek, D.R., & Bureau, M. 2005, ApJ, 633, 154
Schlegel, D.J., Finkbeiner, D.P., & Davis, M. 1998, ApJ, 500, 525
Seth, A.C., Dalcanton, J.J., Hodge, P.W., & Debattista, V.P. 2006, ArXiv Astrophysics e-prints, arXiv:astro-ph/0606066
Shapley, H. 1943, Galaxies (3rd edition) (Harvard University Press: Cambridge)
Sirianni, M., et al. 2005, PASP, 117, 1049
Sivakoff, G.R., Jordán, A., Sarazin, C.L., Blakeslee, J.P., Côté, P., Ferrarese, L., Juett, A.M., Mei, S., & Peng, E.W. 2006, ApJ, in press (`astro-ph/0611237`)
Smith, R.J., Lucey, J.R., Hudson, M.J., Schlegel, D.J., & Davies, R.L. 2000, MNRAS, 313, 469
Tonry, J.L. 1991, ApJ, 373, L1
Tonry, J.L., & Schneider, D.P. 1988, AJ, 96, 807
Tonry, J.L., Ajhar, E.A., & Luppino, G.A. 1989, ApJ, 346, L57
Tonry, J.L., Ajhar, E.A., & Luppino, G.A. 1990, AJ, 100, 1416
Tonry, J. L., Blakeslee, J. P., Ajhar, E. A., & Dressler, A., 1997, ApJ, 475, 399
Tonry, J. L., Blakeslee, J. P., Ajhar, E. A., & Dressler, A., 2000, ApJ, 530, 625
Tonry, J.L., Dressler, A., Blakeslee, J.P., Ajhar, E.A., Fletcher, A.B., Luppino, G.A., Metzger, M.R., & Moore, C.B. 2001, ApJ, 546, 681
Walcher, C. J., et al. 2005, ApJ, 618, 237
Wehner, E. H., & Harris, W. E. 2006, ApJ, 644, L17
White, R.L. 2006, STScI Instrument Science Report ACS 2006-05